

# Synthesis and characterization of ammonia strengthened and ambient dried N-doped hydrophilic graphene aerogel with good electrical conductivity

Feng Xiong<sup>a</sup>, Jiabin Wang<sup>a</sup>, Neville Dickman<sup>a</sup>, Yujing Liu<sup>a,1</sup>, Michael R.C. Hunt<sup>b</sup> and

Lidija Šiller<sup>a,\*</sup>

<sup>a</sup> School of Engineering, Newcastle University, Newcastle upon Tyne, NE1 7RU, UK

<sup>b</sup> Department of Physics, Durham University, Durham, DH1 3LE, UK

<sup>1</sup> current adress: Ugelstad Laboratory, Department of Chemical Engineering, Norwegian

University of Science and Technology (NTNU), 7491 Trondheim, Norway

\*Corresponding author: Lidija.Siller@ncl.ac.uk

## Abstract

We present a novel ‘one-pot’ approach for strengthening reduced graphene oxide (rGO) hydrogels by nitrogen doping. Ammonia is directly added to the precursor reaction mixture prior to hydrothermal gel formation, as opposed to treating as-synthesised rGO hydrogel by ammonia in a second hydrothermal process. This process ensures that the resulting hydrogels are sufficiently robust that aerogels may then be produced by natural drying under ambient temperature and pressure. The as-formed rGO aerogel possesses a Young’s modulus as high as 28 kPa and exhibits superelasticity, withstanding strains of up to 95%. Moreover, the strengthened graphene aerogel possesses an electrical conductivity of  $1.5 \text{ S cm}^{-1}$  and a specific surface area of  $280.0 \text{ m}^2 \text{ g}^{-1}$ . Although the rGO aerogel was sufficiently reduced to provide good electrical conductivity, it retains a water contact angle of  $47 \pm 1^\circ$ , indicating hydrophilic behaviour.

## Keywords

Graphene aerogel, Graphene oxide, hydrothermal synthesis, electrical conductivity, ambient pressure drying.

## 1 Introduction

Aerogels produced from reduced graphene oxide (rGO) – often simply termed graphene aerogels (GA) – are three-dimensional structures which consist of interconnected microsheets and nanosheets of reduced graphene oxide assembled into a hierarchical pore structure and span multiple lengthscales from the microscopic to the macroscopic. GAs are characterised by their high porosity and low density which makes them suitable for applications such as the mitigation of organic pollution in water [1] or use as a three-dimensional framework for battery anodes to accommodate volume fluctuations during charging and discharging [2]. GA is usually hydrophilic as-produced, hence hydrophobic graphene aerogels with a high level of oil adsorption have been synthesized through the calcination of GA in a nitrogen environment, eliminating polar surface oxygen groups [1]. In contrast, enhanced hydrophilicity has been found to facilitate development of exoelectrogenic biofilms in microbial fuel cells, resulting in a decreased start-up period for these systems [2].

Appropriate mechanical properties are crucial in several applications – in particular, cycling compressibility is required for both removal of absorbed species in pollution remediation and supporting volume change in electrochemical energy storage applications. By treating reduced graphene oxide hydrogel with ammonia for an hour at 90 °C, ammonia can react with the oxygen groups on the surface of the rGO and strengthen both the mechanical [3] and electrochemical properties of the resulting GA [4]. N-doped graphene sheets are created as a result of this method, and they have an advantage over undoped graphene sheets in terms of specific capacity as lithium-ion battery (LIB) anodes, reaching 684 mAh g<sup>-1</sup> after 500 cycles [5]. In addition, the three-dimensional graphene aerogel framework offers substantial support for silicon-based and phosphorus-based composite anodes of lithium-ion batteries. For example, Chen and co-workers utilised a porous graphene aerogel-wrapped silicon composite as the anode for lithium-ion batteries which possessed good cyclic stability, achieving a specific capacity of 850 mAh g<sup>-1</sup> after 200 cycles with a coulombic efficiency of 99% at a current density of 0.5 C [6]. Similarly, Wang *et al.* used a graphene aerogel, phosphorus and silicon composite as an anode for lithium-ion batteries. This anode showed a specific capacity of 1094 mAh g<sup>-1</sup> at a current density of 0.5C, with a capacity retention of 80.3% over 200 cycles in half-cell testing [7].

The selection of an appropriate drying procedure is crucial to prevent volume shrinkage and structural cracking when producing monoliths of GA. Supercritical drying [8] and freeze-

drying [9] are techniques commonly employed in preparation of GA, however, these approaches necessitate the use of significant amounts of energy, time and specialized equipment, which leads to high production costs and impedes their large-scale manufacture [10]. The “natural drying” technique, conducted under ambient pressure and temperature, is a cost-effective, energy-efficient, and straightforward alternative, which is therefore highly attractive. Application of natural drying to form GA is usually hindered due to the lack sufficient of strength to endure the capillary forces resulting from solvent evaporation under standard room temperature and pressure conditions [11] and, in consequence, a secondary hydrothermal treatment with ammonia solution has been previously utilised to improve hydrogel properties prior to drying.

In this work a single-step ‘one-pot’ strategy has been adopted for the production of hydrophilic GA with high electrical conductivity, elasticity and mechanical durability. Ammonia solution was directly added to the precursor mixture prior to gelification through hydrothermal treatment instead of using a second hydrothermal treatment once the gel had formed [11]. The resulting hydrogel was naturally dried under ambient pressure and temperature to form the aerogel. This use of ammonia in the precursor not only streamlines the process but also enhances negative charge on the surface of the rGO sheets, facilitating better dispersion.

## **2 Experimental**

### **2.1 Raw material**

All chemicals were used as received without further purification.  $\text{H}_2\text{SO}_4$  (98%),  $\text{KMnO}_4$  (99%), graphite flakes (99%),  $\text{H}_3\text{PO}_4$  (85%) and ethylenediamine (99%) were purchased from Sigma-Aldrich with ammonia solution (35%w/w) and ethanol (99.8%) purchased from Fisher Scientific. Spectra/Por 1 Dialysis Kits (6-8 kD MWCO) were purchased from Repligen.

### **2.2 Preparation of graphene oxide (GO)**

Graphene oxide was synthesised by the modified Hummers’ method [12].  $\text{KMnO}_4$  (8 g) and graphite (3 g) were gradually added to a mixture consisting of  $\text{H}_3\text{PO}_4$  (20 ml) and  $\text{H}_2\text{SO}_4$  (100 ml), and then stirred continuously three days at 120 rpm rotation speed under ambient conditions.  $\text{H}_2\text{O}_2$  was then slowly added dropwise into the mixture until the colour had been observed to change to a bright yellow. The resulting mixture was then filtered and washed using a Spectra/Por 1 Dialysis Kit with deionised water for approximately two weeks until the pH reached 7. The obtained GO was subsequently dried at 60 °C overnight and characterised by X-ray diffraction (XRD).

### **2.3 Synthesis of ammonia strengthened rGO aerogels by ambient pressure drying**

The hydrothermal approach was employed for the synthesis of rGO hydrogels (GH). In work reported by Xu and co workers [13] the reaction between 1  $\mu\text{L}$  of ethylenediamine (EDA) and 1 mg of graphene oxide (GO) results in the formation of graphene aerogel (GA) which can be naturally dried with little volume reduction. In this study, a volume of 200  $\mu\text{L}$  of EDA solution was added to a 20 ml of a GO suspension with a concentration of 10 mg  $\text{ml}^{-1}$ . The mixture was treated ultrasonically using a Sonoprobe (Sonopuls Ultrasonic Homogenizer) for a duration of 5 minutes. To optimise the composition of the precursor solution varying quantities of 35% ammonia solution (0  $\mu\text{L}$ , 25  $\mu\text{L}$ , 50  $\mu\text{L}$ , 75  $\mu\text{L}$ , 100  $\mu\text{L}$ ) were added prior to gelation. The precursors were enclosed within a Teflon-lined stainless-steel autoclave with a volume of 40 ml and held at a temperature of 140  $^{\circ}\text{C}$  in muffle furnace for 12 hours. Following heat treatment, the resulting hydrothermally produced GH samples were removed from the autoclave and immersed in a 1 wt% ethanol solution for a duration of 6 hours in order to reduce the re-stacking of graphene during the subsequent drying procedure. The GH was then subjected to pre-freezing at a temperature of -18  $^{\circ}\text{C}$  in a commercial freezer for a duration of 8 hours. GA was produced from the resulting GH by ambient pressure drying for a duration of 24 hours at room temperature. Samples are designated GA, GA-25, GA-50, GA-75, and GA-100, with the numerical suffix indicating the quantity of ammonia (in  $\mu\text{L}$ ) introduced during the synthesis.

### **2.4 Materials characterisation and mechanical testing**

The surface morphology of the GA samples was studied using a Zeiss EVO 10 scanning electron microscope (SEM) located at the G.J. Russell Microscopy Facility, Durham University, using a beam energy of 20 keV and secondary electron detection. All other characterisation was undertaken at Newcastle University. XRD employed a Bruker D2 PHASER diffractometer, and it was used to determine the phase structure of the samples. A Hiden Isochema IGA surface area analyser was used to measure  $\text{N}_2$  adsorption/desorption isotherms using Brunauer-Emmett-Teller (BET) theory to calculate specific surface area using partial pressures,  $P/P_0$ , in the range of 0.05 – 0.3 of the adsorption curve of the isotherm. X-ray photoemission spectroscopy (XPS) analysis was conducted by using a K-alpha (Thermo Scientific, East Grinstead, UK) X-ray photoelectron spectrometer. Spectra were acquired using a monochromatic Al  $K\alpha$  X-ray source (1486.6 eV) with a maximum X-ray spot size of 400  $\mu\text{m}$ . Surface charge compensation was achieved with a low energy dual-beam electron/ion flood gun. High resolution spectra of the C 1s line were collected at 40 eV pass energy with a 0.05 eV

step size. Spectral analysis was carried out using Casa XPS (Casa XPS Ltd. Teignmouth, UK). Raman spectroscopy was undertaken at the SAgE Analytical Facility, Newcastle University using a Jobin Yvon LabRam HR-800 (with Argon laser as excitation source at 514 nm). Compression tests were performed using a Tinius Olsen H25 universal testing machine.

### 3 Results and Discussion

Addition of ammonia solution to the rGO/EDA mixture is observed to lead to a considerable lowering of its viscosity (Supporting Material, Videos 1 and 2), which can be understood by the ammonia improving the dispersion of the graphene oxide sheets within the suspension. Adding the ammonia solution causes the surface of the GO sheets to acquire a negative charge, leading to repulsion between them and hence improved dispersion in solution [14, 15]. Figure 1 present images of a rGO hydrogel produced with the addition of 100  $\mu$ L of ammonia solution (Figure 1 (a and c)) and the GA-100 derived from it (Figure 1 (b and d)). It can be seen that in drying the hydrogel to form the GA capillary forces do not result in any significant reduction in volume under natural ambient pressure drying conditions. This phenomenon can be understood by recognising that the volume of water within the GH increases during the freezing step. Consequently, rGO sheets are squeezed together, increasing re-stacking, which leads to the formation of thicker gel walls which increases both the strength and the radii of the gel pores [16]. If the pores within the gel are considered to be cylinders the Young-Laplace equation relates the capillary pressure ( $P$ ) to the solvent surface tension,  $\gamma$ , the contact angle between liquid and surface,  $\theta$ , and the pore surface radius,  $R$ , as [17]:

$$P = \frac{2\gamma\cos\theta}{R}. \quad (1)$$

Therefore, after freezing the initial hydrogel, the capillary pressure is lowered, so that the gels do not collapse upon drying.

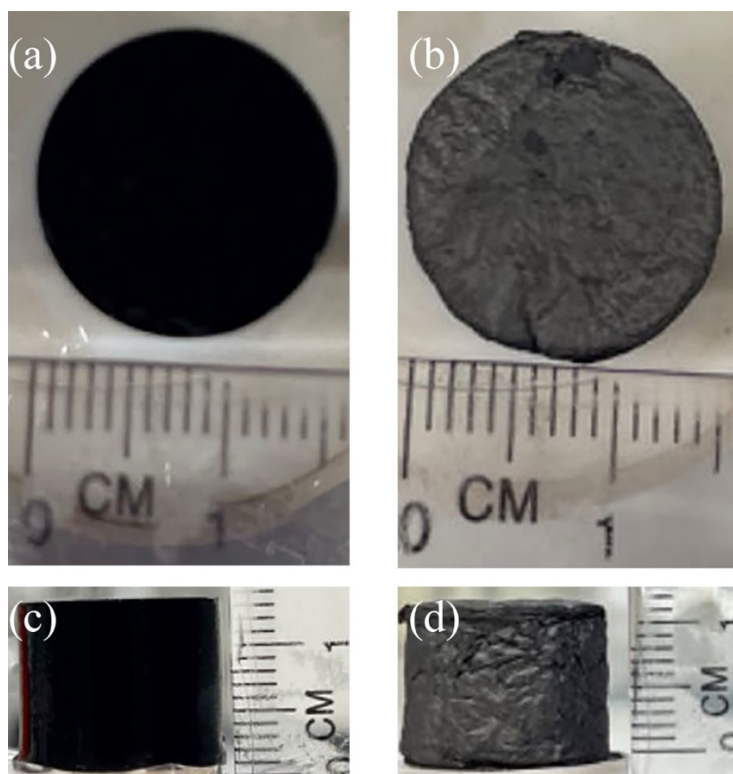


**Fig. 1.** (a, c) rGO hydrogel with 100  $\mu$ L of ammonia solution; (b, d) rGO aerogel formed by drying hydrogel (GA-100).

The structural and chemical composition of the GA was characterised by XRD, Raman spectroscopy, XPS and BET. XRD data from the GO, and rGO aerogels produced with differing ammonia concentrations, are presented in Figure 2. The diffraction peak observed in the GO diffraction scan at a  $2\theta$  angle of  $\approx 10^\circ$  corresponds to an interlayer spacing of 0.847 nm, confirming successful oxidation of graphite [18]. In contrast, there are no strong diffraction peaks seen in GA (Figure 2, red line), indicating exfoliation of the rGO platelets within this material. Hu and co-workers [18] have observed similar behaviour whereas Huang *et al.* [19] report clear diffraction peaks at  $23.6^\circ$ , which can be related to differences in the GO preparation process. When compared with the traditional Hummers' method, the oxygen concentration of graphene oxide prepared via the modified Hummers' method is higher [20]. In consequence, the GA produced from GO prepared via the improved Hummers' method presents clear amorphous structure. GA samples synthesised from gels containing ammonia solution present a clear diffraction peak at  $26.2^\circ$  (corresponding to a  $d$ -spacing of 0.337 nm, characteristic of graphite), indicating that ammonia promotes development of graphitic structures [18] during the aerogel synthesis process.

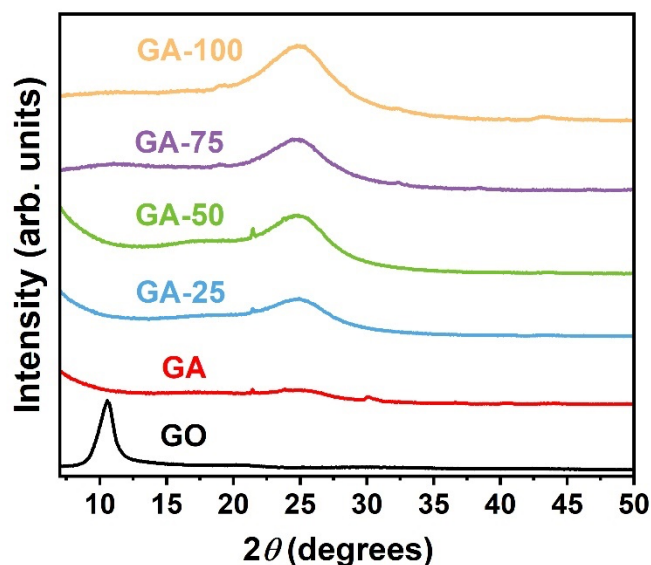


**Fig. 2.** XRD patterns of GO, GA, GA-25, GA-50, GA-75, GA-100 .

Raman spectra of the GA materials show two distinct lines, characteristic of amorphous carbon and graphitic materials containing defects: the  $G$  band, which is observed at  $1587\text{ cm}^{-1}$  and the  $D$  band at  $1352\text{ cm}^{-1}$ , Figure 3. The ratio of the intensities of the  $D$  and  $G$  bands ( $I_D : I_G$ ) is often employed as a means of comparing the relative concentration of symmetry-breaking defects in graphitic materials [19]. However, care needs to be when considering GO and rGO due to the significant degree of disorder and  $sp^3$  bonding within this material [21]. In particular, although the  $D$  peak becomes Raman-active due to the presence of symmetry-breaking defects within a graphite lattice and initially increases with defect density, it originates from the “breathing” mode of hexagonal carbon rings and, if the presence of such ring structures is reduced it can subsequently decrease at high enough defect densities [22].

In consequence, with the reduction of GO  $sp^2$  hybridization is restored and thereby the ratio  $I_D : I_G$  increases despite a decrease in disorder. The spectra in Figure 3 show that  $I_D : I_G$  monotonically increases from 0.998 in GA to 1.217 for GA-100. In previous work by Han *et al.* [3] using post gelation ammonia treatment of rGO hydrogels the  $I_D : I_G$  ratio barely changed, indicating little to no structural recovery of the rGO sheets. In contrast, in this work, we demonstrate that addition of ammonia to the precursor mixture prior to hydrothermal gelation promotes the reduction of GO with the degree of reduction observed increasing with ammonia content.

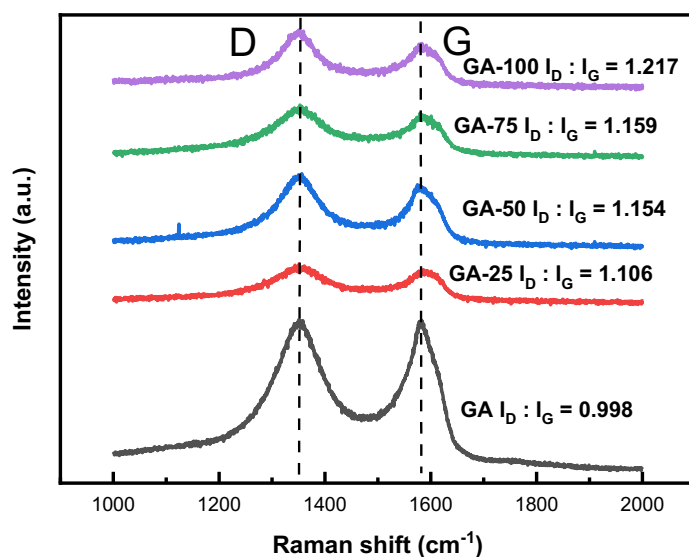


**Figure 3.** Raman spectra of GA, GA-25, GA-50, GA-75, GA-100.

XPS survey spectra and high resolution scans of the C 1s line from GA samples obtained as a function of ammonia solution added to the initial gel precursors are shown in Figure 4. The elemental composition of samples, obtained from the XPS survey spectra, is presented in the Supporting Information in Table S1. An obvious decrease of the oxygen concentration is observed in the survey spectra (Figure 4(a)), with the ratio of carbon to oxygen (C/O) increasing from 5.02 in aerogels produced without ammonia solution to 10.35 at the maximum addition of ammonia solution studied in this work. In accord with the XRD and Raman data discussed above, the conclusion can be drawn that the presence of ammonia in the precursor solution promotes the reduction of graphene oxide during the synthesis of graphene aerogel. The element content obtained from XPS data is presented in the Table S1. The N content in samples is determined to be GA: 4.87 atom%, GA-25: 6.91 atom%, GA-50 7.29 atom%, GA-75: 7.92 atom% and GA-100: 8.09 atom%, correlating with the decrease in oxidation of the rGO, with the nitrogen in the GA sample originating from the EDA in the precursor.

High resolution C 1s XPS data are shown in Figure 4 (b-f). An asymmetric line with binding energy of  $284.6 \pm 0.1$  eV dominates the signal in each sample and corresponds to the presence of  $sp^2$  bound graphitic carbon [20, 23 - 25]. The remaining peaks correspond to C-O at  $286.0 \pm 0.1$  eV [15] (which may overlap with the C-N functionality reported to have a binding energy of  $285.7 \pm 0.1$  eV [26] and C-NH<sub>2</sub> at  $286.2 \pm 0.1$  eV[27] C=O at  $288.0 \pm 0.1$  eV [25, 28], O-C=O at  $288.6 \pm 0.1$  eV [29] and  $\pi$  plasmon at  $290.2 \pm 0.1$  eV [25]. As shown in Figure 4 (b, c,

d and e), the peak of O=C=O disappeared after the ammonia is added into the solution, indicating that these functional groups, in particular, are preferentially reduced in the presence of ammonia solution.

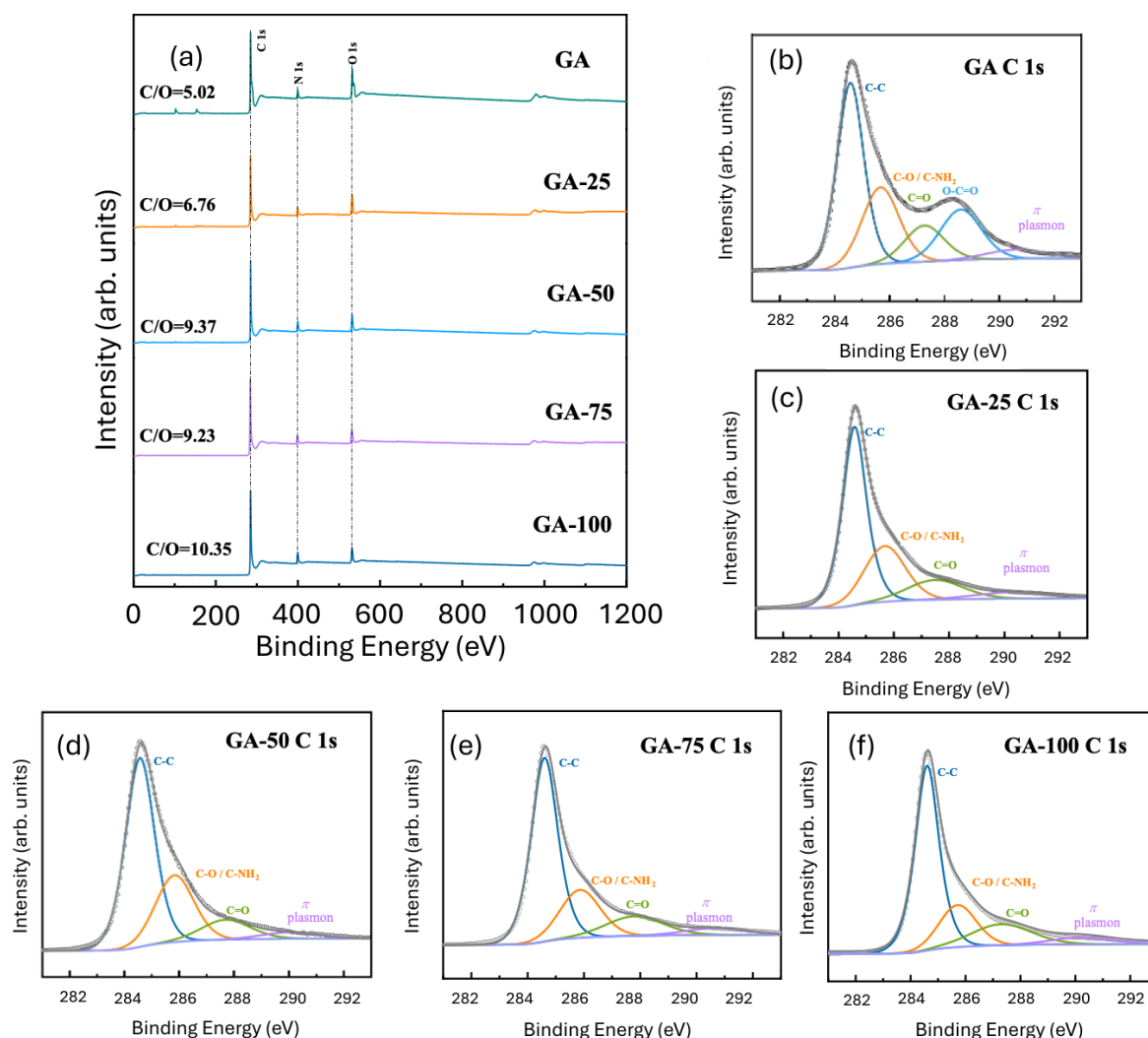


**Fig. 4.** (a) XPS survey scan of all samples. C 1s photoelectron spectra of: (b) GA; (c) GA-25; (d) GA-50; (e) GA-75; (f) GA-100;

Cyclic stress-strain curves for a GA-100 sample with up to 50% of a strain are presented in figure 5(a). They show that the hysteresis loop contracts during the second cycle and then essentially stays the same for the following cycles. The Young's modulus during the first cycle is found to be  $\sim 28$  kPa and decreases non-linearly with cycling, retaining a value of 21.2 kPa after 50 cycles (figure 5 (b)). These high values indicate why the capillary pressures caused by solvent evaporation during the natural ambient pressure drying process do not cause collapse

of the gel. Figure 5(c) presents stress-strain curves measured for the GA-100 sample with strains of 95% and Figure 5(d) shows the recovery height of the same sample. The ultimate stress a GA-100 sample can achieve is  $\sim 0.32$  MPa and the recovery height is found to remain constant (98%) for 10 cycles, indicating that GA-100 possesses excellent reversible compressive deformability. The GA prepared by the simple ‘one-pot’ process outlined in this study compares well with similar aerogels prepared through multi-step processes combining both cross-linking and bridging method and hydrothermal method [13]. Stress-strain curves for up to 95% strain are shown in Figure 5(e) for samples as a function of ammonia solution content during synthesis. The sample produced without addition of ammonia solution, GA, cracks readily during the compression process with the result that stress-strain curves cannot be measured. The fragility of the sample produced without addition of ammonia solution, coupled with the observation that the sample produced with highest amount of added ammonia can withstand the highest stress, indicates that increased rGO reduction, hence  $sp^2$  bonding [18], and incorporation of covalently-bound nitrogen [3] improves the strength and recovery of rGO-based aerogels.

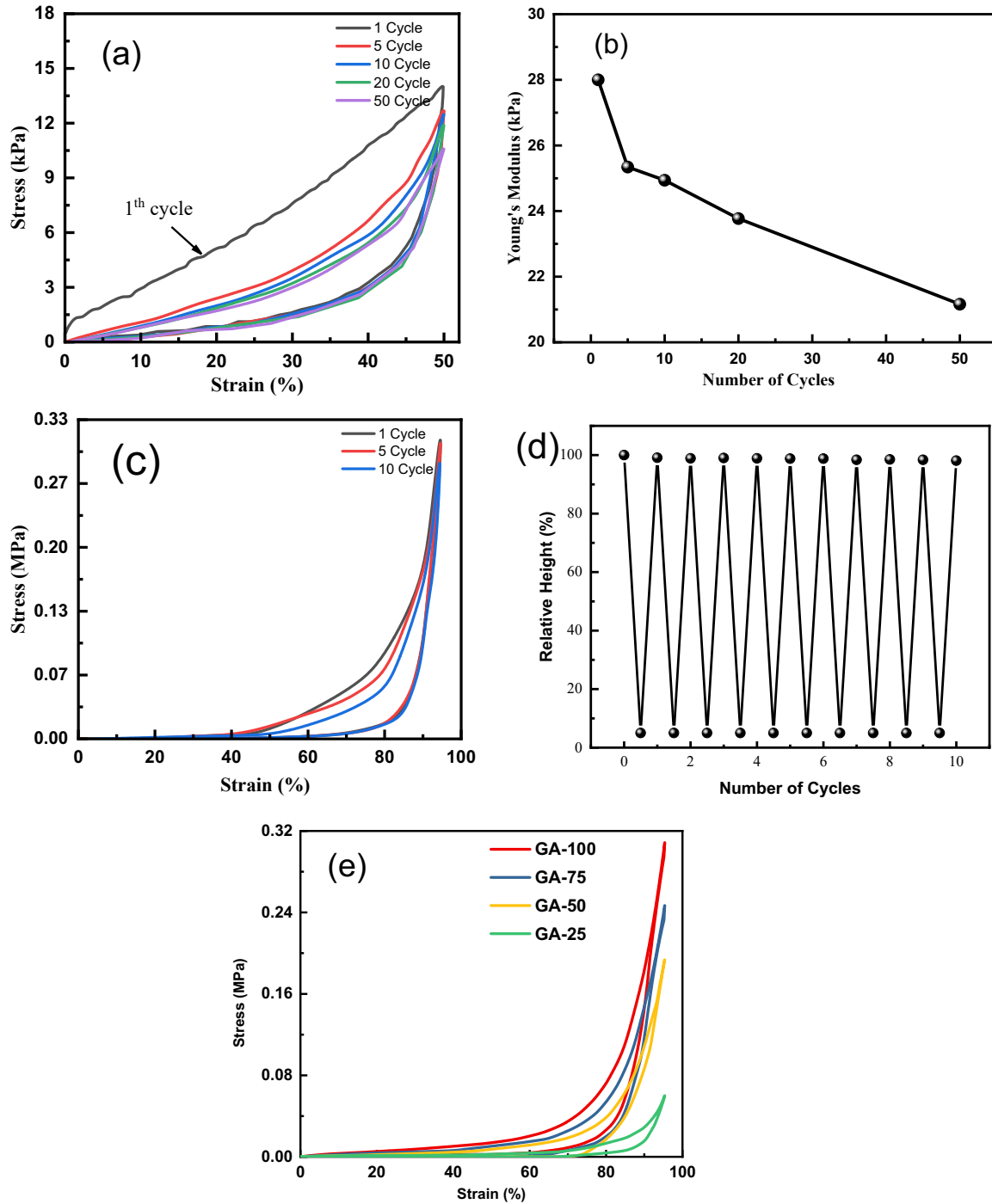


**Fig. 5.** (a) Stress–strain curves of GA-100 up to 50% strain; (b) Corresponding Young's moduli as a function of the number of compression cycles; (c) Stress–strain curves of GA-100 up to 95% strain; (d) The variation of height as a function of cycle numbers for GA-100; (e) Stress–strain curves of all samples, GA-100, GA-75, GA-50 and GA-25 with up to 95% strain in the first cycle.

The hierarchical structure of GA-100 is shown in the SEM micrograph presented in Figure 6 (a). The observed structure is similar to studies which employed ambient pressure drying to obtain graphene aerogels [16, 30]. Figure 6 (b-d) shows higher magnification of SEM images of GA, GA-50, GA-100. It is clear that the surface of the aerogel becomes smoother and less fractured upon increasing addition of ammonia. We suggest two possible reasons for this observation: during the hydrothermal reaction, a portion of the ammonia in solution may convert into ammonia gas, resulting in bubble formation that alleviates surface wrinkles on graphene oxide and consequently enhances its mechanical strength, as shown in the SEM images. This is consistent with previous research [31, 32] which demonstrated that a significant enhancement in the mechanical strength of graphene occurs when surface wrinkles are minimized. Improved mechanical behaviour can also be understood by the enhanced reduction of rGO sheets within the aerogel, as evidenced XRD, Raman spectroscopy and XPS. An increase in the relative area of  $sp^2$ , as opposed to  $sp^3$ , bound carbon reduces brittleness and as the rGO becomes more 'graphitic' we can expect its Young's modulus to tend towards the exceptional values observed in pristine graphene [33].

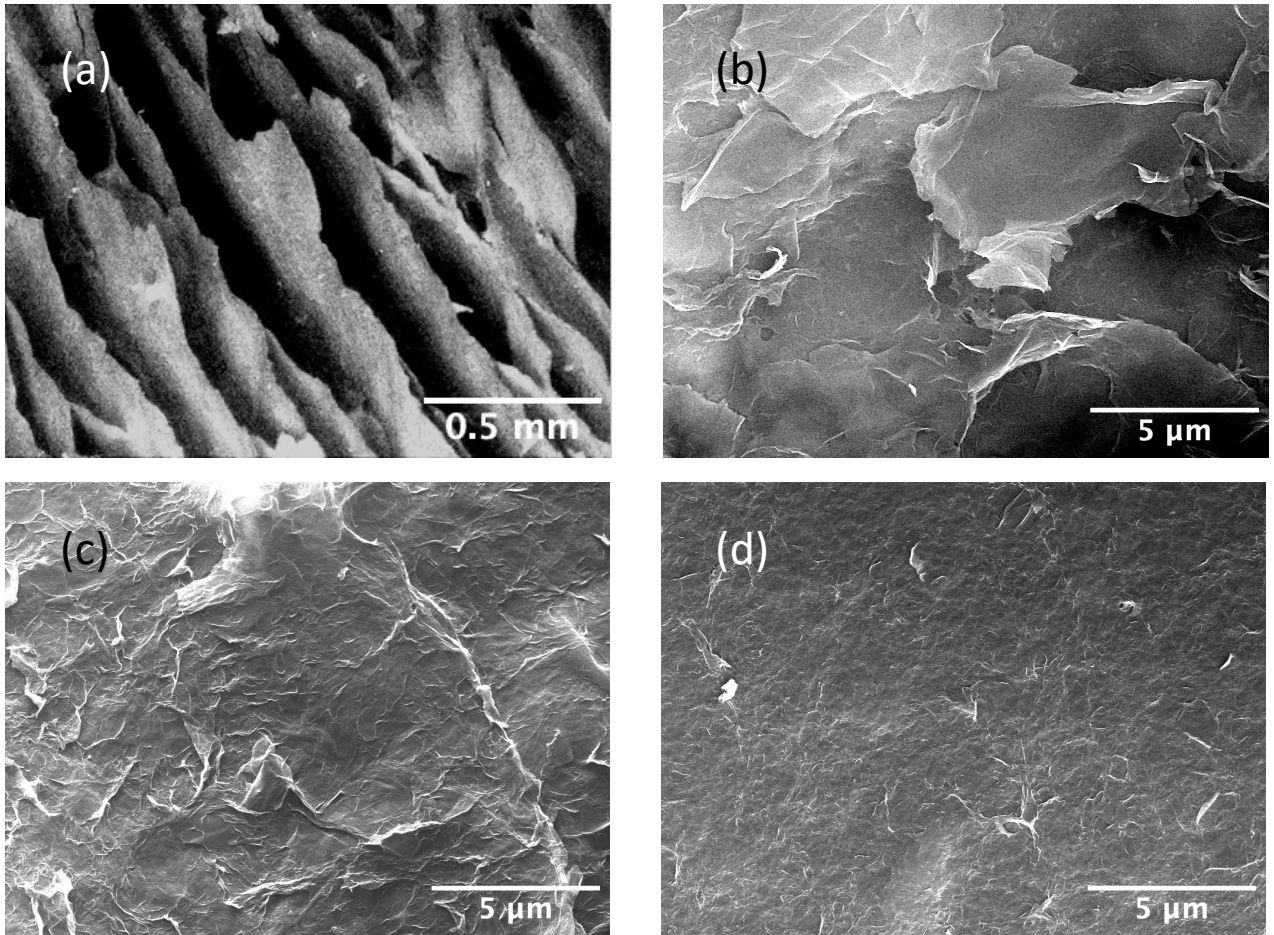


**Fig. 6.** SEM images of: (a) GA-100 at low magnification; (b) GA; (c) GA-50; (d) GA-100 at higher magnification.

Water contact angles measured for GA, GA-50 and GA-100 are presented in Figures 7 (a-c) indicating that all samples are hydrophilic, irrespective of ammonia addition. This contrasts with the results obtained by Huang and co-workers for aerogels produced by post-gelation hydrothermal treatment with ammonia solution, which were observed to be hydrophobic [19]. Although an increase in contact angle with increasing ammonia concentration is observed in our work, indicative of increasing reduction of the rGO sheets within the gel, sufficient concentration of polar surface groups remain to preserve hydrophilic behaviour.

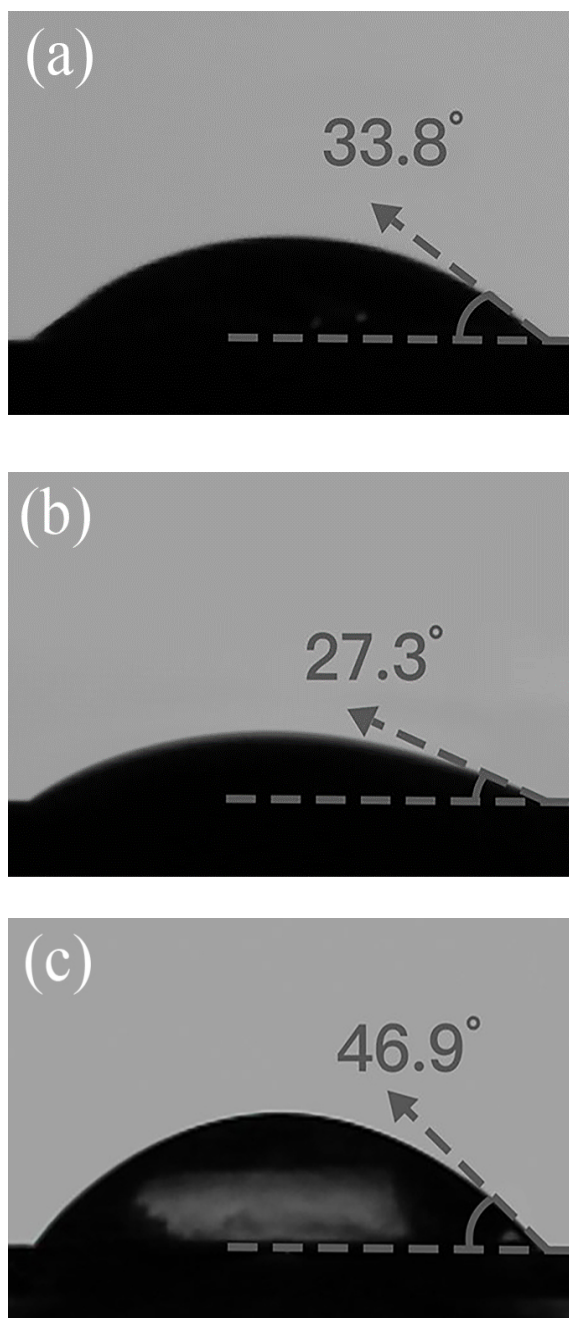


**Fig. 7.** Water contact angle measured on (a) GA; (b) GA-50; (c) GA-100.

Table 1 reports the specific surface area of all samples, obtained from nitrogen absorption isotherms, which shows that the specific area of GA increases with more ammonia addition. The EDA reduces the GO to rGO, but when 25  $\mu\text{L}$  ammonia is added, all ammonia are likely to react with the carboxy groups of GO sheets. The negatively charged surface of graphene oxide sheets enhances electrostatic repulsion, so the aggregation and stacking of graphene sheets is reduced, and therefore the specific surface area of sample increases slightly. When

more (50  $\mu\text{L}$ ) of ammonia is added, ammonia partially reacts with epoxy groups and produces new hydroxy groups. These hydroxy groups might further remove residual EDA groups on surface, and therefore the reduction of GO is higher which strengthens mechanical properties. When 75  $\mu\text{L}$  of ammonia is added, there is enough residual ammonia after removal of the EDA to react with graphene sheets to form covalent bonds which further strengthen the GA. With more ammonia added, nonreacted residual ammonia might transform to gas bubbles inside the gel (in porous structures under high temperature ammonia in solution will transfer to gas). Similar studies with bicarbonates, have observed bubble formation which supports the porous structure from inside during the drying process [17, 34]. This may explain why GA-100 in this work has achieved higher specific area ( $280.0 \text{ m}^2 \text{ g}^{-1}$ ) when compared with other studies of synthesis of GA via ambient pressure drying method (for example, reported surface areas of GA have been  $160 \text{ m}^2 \text{ g}^{-1}$  [13] and  $30 \text{ m}^2 \text{ g}^{-1}$  [35]).

**Table 1.** BET specific surface area of all samples.

| Samples   | GA | GA-25 | GA-50 | GA-75 | GA-100 |
|---|----|-------|-------|-------|--------|
| Specific surface area ( $\text{m}^2 \text{ g}^{-1}$ ) | 43 | 59    | 139   | 211   | 280    |

The current-voltage ( $I$ - $V$ ) characteristics of selected samples are shown in Figure 8. In each case the  $I$ - $V$  characteristic is ohmic, indicating metallic behaviour within the aerogels and enabling their electrical conductivity to be determined. GA-100 presents an excellent electrical conductivity of  $1.5 \text{ S cm}^{-1}$ , greater than the value of  $1.3 \text{ S cm}^{-1}$  reported by Xu *et al.* [13]. Electrical conductivity is found to decrease to  $1.1 \text{ S cm}^{-1}$  for GA-50 and  $0.5 \text{ S cm}^{-1}$  in GA, reflecting the increased oxygen content in these samples. The coupling of a high degree of conductivity with retention of sufficient surface functional groups to maintain hydrophilic behaviour suggests that the aerogels produced in this work may be especially useful as electrodes in aqueous batteries and supercapacitors by promoting wetting which has shown to improve performance in carbon-based electrode materials through the alternative route of addition of surfactants [36].

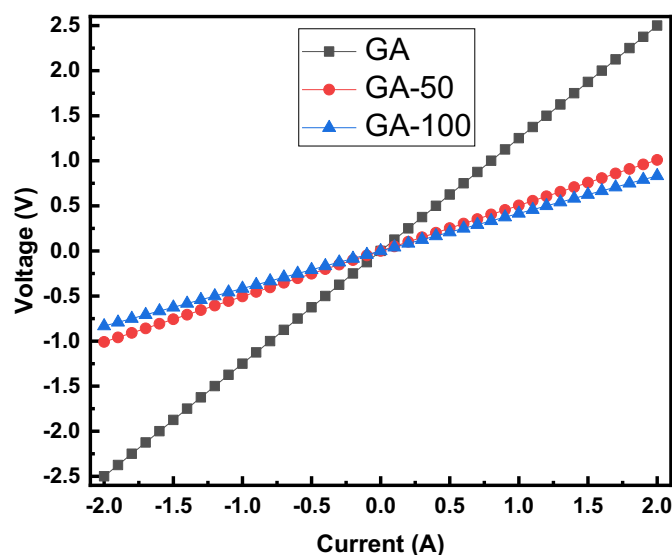


**Fig. 8.** *I-V* curves measured for GA with different ammonia treatments.

#### 4 Conclusion

In this work reduced graphene oxide aerogels strengthened by ammonia were synthesised by a novel ‘one-pot’ hydrothermal technique, avoiding the need for post-gelation treatment. The resulting aerogels showed negligible volume shrinkage when prepared via a natural ambient drying route and retained both good hydrophilicity and electrical conductivity (up to  $1.5 \text{ S cm}^{-1}$ ). Samples prepared with the highest ammonia concentration studied demonstrated excellent mechanical strength, with a Young’s modulus of up to  $\sim 28 \text{ kPa}$ , and excellent retention of mechanical behaviour upon cycling. Although adding ammonia lowers the hydrophilicity, all ammonia treated reduced graphene oxide aerogels remained hydrophilic with GA-100 showing the largest water contact angle of  $47 \pm 1^\circ$ . A mechanism regarding how ammonia strengthens the graphene aerogel is proposed. The hydroxyl ion formed from ammonia reacts with GO sheets which removes EDA that is attached to the GO sheets, which then restores the  $\text{sp}^2$  hybrid structure which is responsible for excellent mechanical properties and excellent electrical conductivity of graphene. The residual ammonia can also form covalent bonds on the graphene sheet surface to further enhance the mechanical strength. Compared with previously reported studies, addition of ammonia prior to the gelation step provides a low-cost and efficient route for the production of reduced graphene oxide aerogels with excellent mechanical and electrical performance.

## **CRedit authorship contribution statement**

**Feng Xiong**: Writing – original draft, Conceptualization, Methodology, Investigation, Data curation. **Jiabin Wang**: Methodology, Data Curation, Investigation, Resources, Writing – review and editing. **Neville Dickman**: Methodology, Formal Analysis, Data curation. **Yujing Liu**: Investigation, Methodology, Formal Analysis, Data Curation. **Michael R.C. Hunt**: Investigation, Writing – review and editing. **Lidija Šiller**: Investigation, Supervision, Funding Acquisition, Formal Analysis, Writing – review and editing.

## **Declaration of competing interest**

The authors declare that they have no known competing financial interests or personal relationships that could have appeared to influence the work reported in this paper.

## **Data availability**

Data will be made available on request.

## **Acknowledgements**

None

## **References**

- [1] Y. Cheng, P. Xu, W. Zeng, C. Ling, S. Zhao, K. Liao, Y. Sun, A. Zhou, Highly hydrophobic and ultralight graphene aerogel as high efficiency oil absorbent material, *J. Environ. Chem. Eng.* 5 (2017) 1957-1963.
- [2] J. Li, Y. Yu, D. Chen, G. Liu, D. Li, H. S. Lee, Y. Feng, Hydrophilic graphene aerogel anodes enhance the performance of microbial electrochemical systems, *Bioresource Technol.* 304 (2020) 122907.
- [3] Z. Han, Z. Tang, P. Li, G. Yang, Q. Zheng, J. Yang, Ammonia solution strengthened three-dimensional macro-porous graphene aerogel, *Nanoscale* 5 (2013) 5462-5467.
- [4] J. P. Mensing, T. Lomas, A. Tuantranont, Ammonia strengthened graphene/CNT-wrapped polyaniline-nanofiber composites loaded with palladium nanoparticles for coin cell supercapacitors, *Electrochim. Acta* 263 (2018) 17-25.

- [5] X. Li, D. Geng, Y. Zhang, X. Meng, R. Li, X. Sun, Superior cycle stability of nitrogen-doped graphene nanosheets as anodes for lithium ion batteries, *Electrochem. Commun.* 13 (2011) 822-825.
- [6] W. T. Chen, R. Muruganatham, W. R. Liu, Construction of 3D porous graphene aerogel wrapped silicon composite as anode materials for high-efficient lithium-ion storage, *Surf. Coat. Tech.* 434 (2022) 128147.
- [7] H. C. Wang, R. Muruganatham, C. T. Hsieh, W. R. Liu, Electrochemical elucidation of phosphorus-doped and 3D graphene aerogel surface-modified SiO<sub>x</sub> porous nanocomposite electrode material for high-performance lithium-ion batteries, *Electrochim. Acta* 477 (2024) 143775.
- [8] P. Zhang, J. Li, L. Lv, Y. Zhao, L. Qu, Vertically aligned graphene sheets membrane for highly efficient solar thermal generation of clean water, *ACS Nano* 11 (2017) 5087-5093.
- [9] G. Shao, D. A. Hanaor, X. Shen, A. Gurlo, Freeze casting: from low-dimensional building blocks to aligned porous structures-a review of novel materials, methods, and applications, *Adv. Mater.* 32 (2020) 1907176.
- [10] X. Zhao, W. Xu, S. Chen, H. Liu, X. Yan, Y. Bao, Z. Liu, F. Yang, H. Zhang, P. Yu, Fabrication of super-elastic graphene aerogels by ambient pressure drying and application to adsorption of oils, *Chinese J. Chem. Eng.* 47 (2022) 89-97.
- [11] C. Huang, Y. Wang, Y. Cheng, Z. Qi, A. Liu, Q. Deng, N. Hu, Naturally dried superelastic bioinspired graphene aerogel for pressure/stretch sensing and separation, *Compos. Sci. Technol.* 226 (2022) 109549.
- [12] J. Wang, H. Zhang, M. R. Hunt, A. Charles, J. Rang, O. Bretcanu, D. Walker, K. T. Hassan, Y. Sun, L. Šiller, Synthesis and characterisation of reduced graphene oxide/bismuth composite for electrodes in electrochemical energy storage devices, *ChemSusChem* 10 (2017) 363-371.
- [13] X. Xu, Q. Zhang, Y. Yu, W. Chen, H. Hu, H. Li, Naturally dried graphene aerogels with superelasticity and tuneable Poisson's ratio, *Adv. Mater.* 28 (2016) 9223-9230.
- [14] D. Li, M. B. Müller, S. Gilje, R. B. Kaner, G. G. Wallace, Processable aqueous dispersions of graphene nanosheets, *Nat. Nanotechnol.* 3 (2008) 101-105.

- [15] X. Fan, W. Peng, Y. Li, X. Li, S. Wang, G. Zhang, F. Zhang, Deoxygenation of exfoliated graphite oxide under alkaline conditions: a green route to graphene preparation, *Adv. Mater.* 20 (2008) 4490-4493.
- [16] H. Yang, T. Zhang, M. Jiang, Y. Duan, J. Zhang, Ambient pressure dried graphene aerogels with superelasticity and multifunctionality, *J. Mater. Chem. A* 3 (2015) 19268-19272.
- [17] X. Han, K. T. Hassan, A. Harvey, D. Kuliĳer, A. Oila, M. R. Hunt, L. Šiller, Bioinspired synthesis of monolithic and layered aerogels, *Adv. Mater.* 30 (2018) 1706294.
- [18] H. Hu, Z. Zhao, W. Wan, Y. Gogotsi, J. Qiu, Ultralight and highly compressible graphene aerogels, *Adv. Mater.* 25 (2013) 2219-2223.
- [19] J. Huang, H. Liu, S. Chen, C. Ding, Graphene aerogel prepared through double hydrothermal reduction as high-performance oil adsorbent, *Mat. Sci. Eng. B-Adv.* 226 (2017) 141-150.
- [20] N. Yadav, B. Lochab, A comparative study of graphene oxide: Hummers, intermediate and improved method, *Flatchem* 13 (2019) 40-49.
- [21] E. Petrova, S. Tinchev, P. Nikolova, Interference effects on the  $I_D/I_G$  ratio of the Raman spectra of diamond-like carbon thin films. <https://doi.org/10.48550/arXiv.1112.0897>, 2011.
- [22] A.C. Ferrari and J. Robertson, Interpretation of Raman spectra of disordered and amorphous carbon *Phys. Rev. B* 61 (2000) 14095 <https://doi.org/10.1103/PhysRevB.61.14095>
- [23] M. Montalti, S. Krishnamurthy, Y. Chao, Yu. V. Butenko, V.L. Kuznetsov, V.R. Dhanak, M.R.C. Hunt, L. Šiller, Photoemission spectroscopy of clean and potassium-intercalated carbon onions, *Phys. Rev. B.* 67 (2003) 113401.
- [24] A.K. Chakraborty, R.A.J. Woolley, Yu.V. Butenko, V.R Dhanak, L. Šiller and M.R.C. Hunt, A photoelectron spectroscopy study of ion-irradiation induced defects in single-wall carbon nanotubes, *Carbon* 45 (2007) 2744-2750.
- [25] V. Butenko, S. Krishnamurthy, A.K. Chakraborty, V.L. Kuznetsov, V.R. Dhanak, M.R.C. Hunt and L. Šiller, Photoemission study of onionlike carbons produced by annealing nanodiamonds, *Phys. Rev. B* 71 (2005) 075420.

- [26] S. Delpeux, F. Beguin, R. Benoit, R. Erre, N. Manolova, I. Rashkov, Fullerene core star-like polymers-1. Preparation from fullerenes and monoazidopolyethers, *Eur. Polym. J.* 34 (1998) 905-915.
- [27] H. Guo, B. Niu, X. Wu, Y. Zhang, S. Ying. Effective removal of 2, 4, 6-trinitrophenol over hexagonal metal–organic framework NH-MIL-88B (Fe), *Appl. Organomet. Chem.* 33 (2019) e4580.
- [28] D. Rats, L. Vandenbulcke, R. Herbin, R. Benoit, R. Erre, V. Serin, J. Sevely, Characterization of diamond films deposited on titanium and its alloys, *Thin Solid Films* 270 (1995) 177-183.
- [29] J. Zhang, Y. Xu, Z. Liu, W. Yang, J. Liu, A highly conductive porous graphene electrode prepared via in situ reduction of graphene oxide using Cu nanoparticles for the fabrication of high performance supercapacitors, *RSC Adv.* 5 (2015) 54275-54282.
- [30] P.Y. Chen, J. Sodhi, Y. Qiu, T. M. Valentin, R. S. Steinberg, Z. Wang, R. H. Hurt, I. Y. Wong, Multiscale graphene topographies programmed by sequential mechanical deformation, *Adv. Mater.* 28 (2016) 3564-3571.
- [31] P. Li, M. Yang, Y. Liu, H. Qin, J. Liu, Z. Xu, Y. Liu, F. Meng, J. Lin, F. Wang, C. Gao, Continuous crystalline graphene papers with gigapascal strength by intercalation modulated plasticization, *Nat. Commun.* 11 (2020) 2645.
- [32] L. Li, J. Yang, T. Tan, W. Shu, C. J. Low, Z. Zhang, Y. Zhao, C. Li, Y. Zhang, X. Li, H. Zhang, X. Zhao, Z. Kou, Y. Xiao, F. Verpoort, H. Wang, L. Mai, D. He, Large-scale current collectors for regulating heat transfer and enhancing battery safety, *Nat. Chem. Eng.* 1 (2024) 542-551.
- [33] J.-U. Lee, D. Yoon and H. Cheong, Estimation of Young's Modulus of Graphene by Raman Spectroscopy, *Nano Lett.* 12 (2012) 4444-4448 DOI: 10.1021/nl301073q
- [34] J. Lu, J. Wang, K. T. Hassan, A. Talmantaite, Z. Xiao, M.R.C. Hunt, L. Šiller, Morphology control of nickel nanoparticles prepared in situ within silica aerogels produced by novel ambient pressure drying. *Sci. Rep.* 10 (2020) 11743.
- [35] S. Yan, G. Zhang, F. Li, L. Zhang, S. Wang, H. Zhao, Q. Ge, H. Li, Large-area superelastic graphene aerogels based on a room-temperature reduction self-assembly strategy for sensing and particulate matter (PM 2.5 and PM 10) capture, *Nanoscale* 11 (2019) 10372-10380.

[36] K. Fic, G. Lota and E. Frackowiak, “Electrochemical Properties of Supercapacitors Operating in Aqueous Electrolyte with Surfactants”, *Electrochimica Acta* 55 (2010) 7484–7488.



**Citation on deposit:** Xiong, F., Wang, J., Dickman, N., Liu, Y., Hunt, M. R., & Šiller, L. (2025). Synthesis and characterization of ammonia strengthened and ambient dried N-doped hydrophilic graphene aerogel with good electrical conductivity. *Vacuum*, 232, Article 113846. <https://doi.org/10.1016/j.vacuum.2024.113846>

**For final citation and metadata, visit Durham Research Online URL:**

<https://durham-repository.worktribe.com/output/3319352>

**Copyright statement:** This accepted manuscript is licensed under the Creative Commons Attribution 4.0 licence.

<https://creativecommons.org/licenses/by/4.0/>